HHS Public Access

Detectability comparison between a high energy x-ray phase sensitive and mammography systems in imaging phantoms with varying glandular-adipose ratios

Muhammad U Ghani[1], **Molly D Wong**[1], **Di Wu**[1], **Bin Zheng**[1], **Laurie L Fajardo**[2], **Aimin Yan**[3], **Janis Fuh**[3], **Xizeng Wu**[3], and **Hong Liu**[1,*]

[1]Center for Biomedical Engineering and School of Electrical and Computer Engineering, University of Oklahoma, Norman, OK 73019, USA

[2]Department of Radiology and Imaging Sciences, University of Utah, Salt Lake City, UT, 84132, USA

[3]Department of Radiology, University of Alabama at Birmingham, Birmingham, AL, 35249, USA

Abstract

The objective of this study was to demonstrate the potential benefits of using high energy x-rays in comparison with the conventional mammography imaging systems for phase sensitive imaging of breast tissues with varying glandular-adipose ratios.

This study employed two modular phantoms simulating the glandular (G) and adipose (A) breast tissue composition in 50G-50A and 70G-30A percentage densities. Each phantom had a thickness of 5 cm with a contrast detail (CD) test pattern embedded in the middle. For both phantoms, the phase contrast images were acquired using a micro-focus x-ray source operated at 120 kVp and 4.5 mAs, with a magnification factor (M) of 2.5 and a detector with a 50 μm pixel pitch. The mean glandular dose delivered to the 50G-50A and 70G-30A phantom sets were 1.33 and 1.3 mGy, respectively. A phase retrieval algorithm based on the phase attenuation duality (PAD) that required only a single phase contrast image was applied. Conventional low energy mammography images were acquired using GE Senographe DS and Hologic Selenia systems utilizing their automatic exposure control (AEC) settings. In addition, the automatic contrast mode (CNT) was also used for the acquisition with the GE system. The AEC mode applied higher dose settings for the 70G-30A phantom set. As compared to the phase contrast images, the dose levels for the AEC mode acquired images were similar while the dose levels for the CNT mode were almost double.

The observer study, contrast-to-noise ratio (CNR) and figure of merit (FOM) comparisons indicated a large improvement with the phase retrieved images in comparison to the AEC mode images acquired with the clinical systems for both density levels. As the glandular composition increased, the detectability of smaller discs decreased with the clinical systems, particularly with the GE system, even at higher dose settings. As compared to the CNT mode (double dose) images, the observer study also indicated that the phase retrieved images provided similar or improved detection for all disc sizes except for the disk diameters of 2 mm and 1 mm for the 50G-50A phantom and 3 mm and 0.5 mm for the 70G-30A phantom.

---

*liu@ou.edu.

This study demonstrated the potential of utilizing a high energy phase sensitive x-ray imaging system to improve lesion detection and reduce radiation dose when imaging breast tissues with varying glandular compositions.

Keywords

High-energy phase contrast imaging; phase retrieval; breast density; mammography

1. Introduction

Breast cancer is the second leading cause of cancer death in women after lung cancer. Approximately 1 in 8 (12%) women in the US will develop invasive breast cancer during their lifetime [1]. A number of risk factors for breast cancer have been established, including personal and family history. High mammographic breast density has been identified as an independent risk factor for developing breast cancer, with estimates of relative lifetime risk ranging from two to six-fold as compared to non-dense breasts [2–8]. The BI-RADS classification system identifies four classes of breast densities, in order of increasing risk [9, 10]: Class 1, predominantly fatty with less than 25% fibro-glandular tissue; Class 2, scattered fibro-glandular tissues ranging from 25–50% of the breast; Class 3, heterogeneously dense with 50–75% of fibro-glandular tissues; and Class 4, extremely dense with greater than 75% fibro-glandular and fibrous tissue.

The sensitivity of mammography for the detection of breast cancer in non-dense breasts has been reported to be 85% [11]. On the other hand, the sensitivity drops as low as 48% in women with extremely dense breasts, i.e. Class 4 (greater than 75% fibro-glandular tissue) [12, 13]. Screening modalities that are effective for this population of women are crucial for optimal early diagnosis of breast cancers. Additional screening with magnetic resonance (MR) imaging or automated breast ultrasonography (AB US) after screening mammography increases the rate of early detection of breast cancer in women with dense breasts [13,14, 15–18]. Thus, there is room for improvement in screening mammography for the diagnosis of cancer, particularly in dense breast imaging.

Conventional mammography is sensitive to the attenuation coefficients of tissues. Unfortunately, dense breast tissue makes mammograms more difficult to interpret by masking potential tumors, since tumor and dense breast tissue both appear white on a mammogram. Phase sensitive mammography is an innovative and emerging x-ray imaging technique. The in-line phase sensitive approach involves the simplest implementation — provided that the imaging system is spatially coherent — as it does not involve the introduction of any optical element between the sample and detector [19–21]. A micro focus source generates a partially coherent x-ray beam which traverses a sample, and a sample-to-detector distance is introduced for the development of interference patterns on the imaging plane. The phase modulation of the emerging beam is transformed into amplitude modulation, due to the free-space propagation of the x-rays after passing through the object. Contrast is generated from the interference among parts of the emerging wave fronts [21–23] that have experienced different phase shifts (φ). This contrast is superimposed onto the

attenuation contrast on the image and helps to improve the visibility of the borders of structures and other fine details. As reported previously [24], in-line phase contrast imaging faces two key challenges in clinical implementation. The first challenge is to achieve adequate x-ray transverse coherence while providing sufficient photon flux at short exposure times. Micro-focus x-ray sources operating with large source-to-object distances can provide large transverse coherent lengths [20, 21]; however, a very long exposure time is required for imaging due to the limited current of the micro-focus tubes. To address this challenge, a high energy beam of approximately 100–120 kV has been utilized recently to acquire phase sensitive images of soft tissue-equivalent phantoms with shorter exposure time [24, 25]. Secondly, although the interfaces of different tissue areas are greatly accentuated in a phase contrast image, the bulk of the phase contrast in a given tissue area may be lost if the phase shifts vary slowly. In order to fully exhibit tissue phase contrast, one needs to disentangle tissue phase shifts from the combined attenuation/phase contrast in a phase sensitive projection. To address the second challenge, we implemented an effective and radiation dose efficient phase retrieval approach [26–29]. In this study, we compared the detectability of a contrast detail (CD) test pattern embedded in modular breast-simulating phantoms of varying glandular and adipose tissue compositions using the low energy clinical mammography and high energy in-line phase sensitive technique. To the best of our knowledge, a comparison of relative detectability of these two modalities in imaging phantoms with varying glandular compositions has not been previously presented.

2. Methods and Materials

2.1 Phantoms

Two modular phantoms (CIRS Inc, Norfolk, VA, USA) were utilized comprising of multiple homogenous slabs that simulated the glandular (G) and adipose (A) tissue composition of a human breast. The slabs were made of epoxy resins with x-ray attenuation properties similar to various density levels of adipose and glandular densities. The slabs were composed of 50G-50A and 70G-30A percentage densities of the glandular and adipose tissue. Three slabs of similar densities were sandwiched together to create a 5 cm thick phantom with the middle slab having a thickness of 1 cm and the outer slabs each having a thickness of 2 cm, respectively. The middle slab of each phantom was machined to include a contrast detail (CD) test pattern as shown in Figure 1 (a). This pattern consisted of a 6×6 matrix of cylindrical holes with diameters of 0.25, 0.5, 1, 2, 3 and 4.25 mm and depths of 0.1, 0.2, 0.4, 0.6, 0.8 and 1 mm.

2.2 Phase Sensitive X-ray Imaging Prototype

The benchtop inline phase sensitive x-ray imaging prototype has imaging and measurement components mounted on an optical rail, which allows the ability to adjust the source-to-object distance (SOD) and source to image-detector distance (SID) for the desired geometric magnification: $M = SID/SOD$. The schematic diagram of the inline phase sensitive prototype is shown Figure 1 (b). The prototype has a micro focus x-ray source (Model L8121-03, Hamamatsu Photonics, Japan) that consists of a tungsten (W) target and a 200 μm thick Beryllium (Be) output window with tube voltage and tube current ranging from 40–150 kV and 10–500 μA, respectively. The source focal spot size varies from 7–50 μm as the output

power varies from 10–75 W. The focal spot to output window distance (FOD) is 17 mm while the x-ray beam angle is approximately 43 degrees. The prototype incorporates a CMOS flat panel detector (C7942SK-25, Hamamatsu Photonics, Japan) with a pixel pitch of 50 μm, an active area of 120 mm × 120 mm and 12-bit digital output. The geometric magnification used in this study was 2.5, with a SOD = 68 cm and SID = 170 cm. The phase sensitive images were acquired using a tube voltage of 120 kVp, a tube current of 500 μA, and an exposure time of 9 sec (4.5 mAs). A 2.5 mm thick aluminum (Al) filter was utilized to harden the beam and block the low energy photons. These specific acquisition parameters are considered optimal when utilizing high energy x-rays for phase contrast and phase retrieval imaging of soft tissues [30]. The half value layer (HVL) corresponding to these acquisition settings was 4.3 mm Al. The corresponding mean glandular dose (D_g) values utilizing the specified acquisition parameters for the 50G-50A and 70G-30A phantoms were 1.33 and 1.3 mGy, respectively.

2.3 Clinical x-ray imaging system configuration

The conventional mammography systems utilized in this study were a Senographe DS (GE Medical System, USA) and a Selenia (Hologic, Bedford, MA, USA). The Senographe DS utilizes an x-ray tube with dual anode targets of molybdenum (Mo) and rhodium (Rh), and a choice of Mo, Rh and Al filtration. It has an indirect conversion flat panel detector that is coupled with a scintillator of cesium iodide (CsI) doped with thallium (CSI: TI). The detector has a pixel pitch of 100 μm with a pixel array of 2294×1914 that provides a field of view of 22.9 cm×19.1 cm. The Selenia system utilizes a tungsten (W) anode target and a choice of rhodium (Rh) or silver (Ag) filtration. It has an amorphous-selenium (a-Se) flat-panel detector that performs a direct conversion of the incident x-ray photons into electric charge. The detector has a pixel pitch of 70 μm with a pixel array of 4096×3328 that provides a field of view of 28.6 cm×23.3 cm. The source to image-detector distance (SID) for the Senographe is 66 cm, while the Selenia has an SID of 70 cm. Both the systems utilized an anti-scatter grid for scatter rejection.

For both systems, the phantom images were acquired using an automatic exposure control (AEC) setting that automatically selects suitable tube voltage (kV), anode/filter combination, and mAs value (the product of tube current and exposure time) depending on the compressed thickness of the breast and its attenuation to x-ray, as determined by the pre-pulse x-ray exposure. In addition to the AEC mode, an automatic contrast mode (CNT) was also used for the acquisition with the GE system. The CNT mode applied a lower kV and higher mAs values which resulted in dose values that are more than double as compared to the standard AEC mode images. The acquisition parameters used for the imaging are summarized in in Table 1 below.

2.4 Mean Glandular Dose

The formation of cancer (carcinogenesis) occurs in glandular breast tissue and therefore it is the dose within this tissue type that needs to be monitored. The D_g values were calculated as [31–34],

$$D_g = D_{gN}, X_{ESE} \quad (1)$$

where D_{gN} is the normalized average glandular dose coefficient and X_{ESE} is the object entrance exposure. The entrance exposure measurements were obtained with a calibrated ionization chamber and dosimeter. D_{gN} values were determined by experimental and computer simulation methods based on the following factors: radiation beam quality (x-ray energy or HVL), x-ray tube target material, filter material, breast thickness and breast tissue composition. For the 120 kVp beam utilized in this study, the D_{gN} values were computed from the x-ray spectral average of the Monte Carlo simulation-derived values for various photon energies. The x-ray spectrum was measured with an x-ray spectrometer having a $3 \times 3 \times 1$ mm^3 CdTe detector (Amptek Incorporated, Bedford, Massachusetts). The complete detail for calculating D_{gN} can be found elsewhere [24, 33].

2.5 Phase Retrieval Method

In order to fully exhibit the phase-contrast of the disks in the phantom, the phase map of the phantom must be retrieved from its phase sensitive projection. A recently developed phase retrieval method known as phase-attenuation duality (PAD) was used to retrieve the phase map from a single phase sensitive projection of the phantom [26–29]. This method has been applied recently for biomedical applications [24, 25, 35–38].

When the x-ray energy falls within the 60–500 keV range, both soft-tissue (Z<10) attenuation and soft-tissue phase are related to the projected electron density, $\rho_{e,}$. This relationship is referred to as the phase-attenuation duality (PAD). This is because Compton scattering dominates the interaction between the x-rays and the low-Z elements within this photon energy range. When PAD holds, phase shift of the object and x-ray attenuation are related to $\rho_{e,}$ as follows:

$$\phi(\vec{r}) = -\lambda r_e \rho_{e,p}(\vec{r}), \quad A^2 = \exp(-\sigma_{KN} \rho_{e,p}(\vec{r})) \quad (2)$$

With this method, the phase map can be retrieved from just a single phase-sensitive projection,

$$\phi(\vec{r}) = \frac{\lambda r_e}{\sigma_{KN}} . ln \left\{ \left[1 - \left(\frac{\lambda R_2}{2\pi M} . \frac{\lambda r_e}{\sigma_{KN}} . \nabla^2 \right) \right]^{-1} \left(\frac{M^2}{I_{in}} I(\vec{r}_d) \right) \right\} \quad (3)$$

where $\phi(r)$ represents the phase map of the object, λ is the average wavelength of x-ray, σ_{KN} is the Klein-Nishina total cross-section of Compton scattering, and $r_e = 2.818 \times 10^{-15}$ m is the classical electron radius. In addition, $I(\vec{r}_d)$ is the acquired phantom's phase-sensitive intensity at the r_D on the detector, I_{in} is the entrance x-ray intensity, and R_2 and M are the object-to-detector distance and the geometric magnification of the system respectively. Derived from x-ray propagation equations, the operator ∇^2 denotes the two dimensional

transverse Laplacian differential operator, and $\left[1-\left(\frac{\lambda R_2}{2\pi M}\cdot\frac{\lambda r_e}{\sigma_{KN}}\cdot\nabla^2\right)\right]^{-1}$ represents the inverse pseudo-differential operator of the forward differential operator.

The composition of the phantoms that were used in this study are also dominated by low-Z elements, thus the PAD relationship holds when using x-rays with energies ≥60 keV. In utilizing a polychromatic micro focus x-ray tube, it was necessary to approximate the values utilized in Equation (3) for the average wavelength λ and the Klein–Nishina total cross-section σ_{KN} as those corresponding to a 60 keV x-ray beam, which is the approximate average output x-ray energy from a tungsten target tube operating at 120 kVp.

2.6 Analyses and Comparison of the Images

2.6.1 Observer Study—Conducting an observer study using contrast-detail (C-D) analysis is widely accepted as a simple and effective method for comparison of medical imaging systems and techniques including mammography applications [39–43]. All the images were randomly presented to 10 independent highly trained observers for the analyses, which involved each observer identifying the minimum perceptible hole for each diameter in the image. The images were displayed on a high resolution monitor in a dark room. The monitor was calibrated using the DICOM grayscale standard display function. The reading time was unlimited for each observer. C-D curves were generated for each image according to the averaged observers' scores to compare the relative performance of the phase retrieved and conventional clinical images. The C-D curve relates the threshold contrast necessary to perceive an object as a function of the object's diameter. Curves for different systems or techniques can easily be compared, as a system exhibiting higher performance produces a C-D curve located closer to the x-y axis. A student t confidence interval was constructed around each data point for determining the variance among the observers for that point. This study utilized a 95% confidence interval with n − 1 degrees of freedom, where n represents the number of observers.

2.6.2 Contrast-to-noise ratio (CNR) and figure of merit (FOM) evaluations—The use of C-D analyses unites the concepts of spatial resolution and contrast resolution on the same graph. It is excellent in providing the relationships visually but it is not quantitative. For the quantitative comparison of the three different imaging systems, the contrast-to-noise ratios (CNRs) of the disk targets in each phantom were calculated. The CNR of a disk target is defined according to the Rose model as follows [44–46]

$$CNR = \frac{S_A - S_B}{\sqrt{(\sigma_A^2 + \sigma_B^2)/2}} \times \sqrt{a_D/a_p} \quad (4)$$

where S_A denotes the mean pixel value of the disc target averaged over a region of interest (ROI), S_B is the mean pixel value of the background averaged over an ROI of the same size, σ_A^2 and σ_B^2 are the corresponding pixel value variances, and a_D and a_p are the areas of a disk target and a pixel, respectively. The ROI size for the target disks varied with its diameter.

Four ROIs all of equal size, as of ROI of the target disks, were positioned in the background regions around each disk.

The achieved CNR for any given disk also depends on the radiation dose. Since, the three imaging systems utilized different radiation dose levels, hence, we define a figure of merit (FOM) for target disk imaging performances. FOM is a quantity that is used to characterize the performance of a device, system or method, relative to its alternatives and it is given as

$$FOM = CNR^2 \Big/ Dose \quad (5)$$

The CNR for x-ray quantum limited detectors is related to $N^{1/2}$, and since the dose is proportional to N, by squaring CNR the influence of N is eliminated in the above FOM $((N^{1/2})^2 / N = 1)$. This conveniently eliminates the parameter of exposure level from the comparative analyses [47]. Hence, the defined FOM reflects the influence that photon energy has in terms of dose efficiency. We measured the CNR and the FOM values for four target discs in the phantom which were 4.25 and 3 mm in diameter with drilled depths of 1 and 0.8 mm. The phase retrieved and clinical images acquired under the AEC modes with the two clinical units were utilized in the computation of CNR and FOM.

3. Results

3.1 Observer Study

Figure 2 provides the contrast detail images of the phantoms simulating the 50% glandular/ 50% adipose density acquired with the GE, Hologic and prototype phase sensitive imaging systems. Figure 2 (a) is the AEC mode acquired image with the GE system, 2(b) is the AEC mode acquired image with Hologic system, 2(c) is the CNT (double dose) mode image acquired with the GE system, and 2(d) is the phase retrieved image of the phantom. The images acquired with the clinical units were cropped to only include the rectangular regions of identical size surrounding the CD test pattern. Due to the limited size of the CMOS detector and the magnification factor utilized, only the CD pattern of the phantom was captured on the image. With the exception of window/leveling, flat field correction and dark current correction, no image processing methods were applied to the images. Similarly, Figure 3 provides the CD images of the phantoms simulating the 70% glandular/ 30% adipose density acquired with a same sequence of (a)–(d) as of Figure 2. From visual inspection, one can see that the most difficult disks to perceive are in the lower left (smaller with lower contrast), and the easiest disks to perceive are the in upper right (larger with higher contrast) on these phantom images. Furthermore, the phase retrieved image is offering a noticeable improvement in disc detection as compared to the images acquired under similar dose levels with the clinical mammography systems. Hologic acquired AEC images have improved disc detection capability as compared to the GE acquired AEC images.

Figure 4 compares the contrast threshold detection performance of the phase retrieved image with the conventional clinical mode images for the phantoms simulating the 50% glandular/

50% adipose breast tissue. At similar dose levels, the phase retrieved image is superior to the images acquired with the two mammography systems under their AEC modes. One can see clearly on the C-D curve that for all the disc sizes, observers perceived more discs. It is also interesting to note that the AEC image of the Hologic system yields improved detection as compared to the AEC mode of the GE system. When the radiation dose was increased more than twice, the contrast resolution of the image acquired with GE system improved and it outperformed the Hologic AEC mode image for all the discs diameters and the phase retrieved image for the discs with 2 mm and 1 mm diameters. As CNT mode applies higher dose settings—the relative noise in the image is less, and the C-D curve shows that it has better contrast resolution.

Figure 5 provides the contrast threshold detection performance of the phase retrieved image with the conventional clinical mode images for the phantom simulating the 70% glandular/ 30% adipose breast tissue. With the clinical systems, the exposure and dose values both increased for this phantom, as the pre-pulse x-ray beam sensed a different attenuation due to the higher density while traversing the phantom. When acquiring the phase sensitive images of this phantom, the exposure values were maintained at 4.5 mAs to be consistent with the first set of images. Contrary to the clinical systems, the radiation dose for imaging the 70–30 set phantom was less as compared to the 50-50 set. One can see from the C-D curves that the phase retrieved image is superior in detection of all the discs as compared to the clinical images acquired under the AEC mode with similar dose levels. The detection of the large discs is almost the same for the phase retrieved and Hologic acquired images. As the disc diameter decreases, the Hologic acquired image contrast reduces, which results in reduced detection of those discs. The Hologic acquired image outperforms the GE image under the AEC mode. With double dose, the CNT mode of the GE system exhibits improved detection of discs, as it outperforms the phase retrieved image in providing better contrast resolution for the 3 mm and 0.5 mm disks. The noise reduction provided at double dose levels with the CNT mode was not enough to completely offset the phase retrieved image acquired at a low dose.

3.2 CNR and FOM

The superiority of the phase sensitive imaging system as seen in the observer study is further endorsed by its CNR and FOM values. The results provided in Table 2 for the 50G-50A phantom set demonstrate that the ratios of CNR with the phase image to that of the Hologic acquired image ranges from 4.62–5.16. The FOM values calculated for the phase images range from a factor of 22.9–28.53 greater than the FOM values for the Hologic acquired image. Similarly, the ratios of CNR with phase image to that of the GE acquired image ranges from 4.53–5.28 while the ratio of FOM values ranges from 15.9–21.6.

The phase retrieved image has approximately five times the CNR of both the clinical systems images which validates the image quality improvements offered by the phase sensitive imaging system. For example, the disk with 3 mm diameter and 1 mm drilled depth provided the CNR values of 8.37, 1.81 and 1.67 with the phase retrieved, Hologic and GE images. The improvement of CNR with the phase sensitive imaging system directly impacts the FOM ratios with the two clinical systems. As compared to the Hologic system, the dose

with the GE system was less which resulted in higher FOM values which in return yielded a smaller of FOM ratios. For the same disk, the FOM for the Hologic and GE image was 2.30 and 2.70 which resulted in FOM ratios of 22.9 and 19.5 respectively.

Both the clinical systems applied higher dose for adequate image quality for the denser phantom, but we were able to maintain the image quality enhancement without increasing the exposure and dose to the denser phantom. Table 3 provides the CNR and FOM values for the 70G-30A phantom set. The ratios of CNR with the phase image to that of the Hologic acquired image ranges from 4–4.95. The FOM values calculated for the phase images range from a factor of 19.32–29.64 greater than the FOM values for the Hologic acquired image. Similarly, the ratios of CNR with phase image to that of the GE acquired image ranges from 4.41–5.12 while the ratio of FOM values ranges from 17.1–23.06. This comparison has significance since the phase images were acquired at a reduced dose as opposed to the clinical images, yet still provide a noticeable image quality enhancement in terms of CNR and FOM values. Taking the same disc of 3 mm diameter and 1 mm depth, the FOM ratios of phase retrieved to Hologic and GE images are 29.64 and 23.06 which are slightly higher to the FOM values of the 50G-50A phantom set due to an acquisition with less dose. Higher CNR values warrant a good contrast resolution, less relative noise and thus better image quality. Increasing the mean number of photons (N) incident upon a detector and reducing the scatter by employing an anti-scatter grid reduces the relative noise and improves the contrast resolution. One can see from figure 2 and 3 that the disks offer a much stronger signal with the phase retrieved image as compared to the two opposing images. It is worth to mention that the boundaries of the disks are sharper with the phase retrieved image. It is a well-known fact that with the employment of geometric magnification in clinical radiology, the boundaries of tissues are obscured due to the blurring caused by the finite focal spot size of the x-ray tubes. Phase contrast imaging technique demonstrate the edge enhancement effect at the interfaces of different tissues or materials while providing additional CNR for the diagnostic purposes.

4. Discussion

This study demonstrates the potential benefits of using high energy x-rays for phase sensitive breast imaging. The clinical systems both have different x-ray tube targets and filter settings; hence we cannot apply the same tube current (mA) and exposure time (s) settings. For a fair comparison, we allowed both systems to apply their own optimized techniques, determined by their automatic exposure control (AEC) settings. With increasing breast density, the AEC modes of the two mammography systems selected higher mAs values, based on the attenuation to x-ray determined by the pre-pulse x-ray exposure. This increase in mAs resulted in higher dose levels, which in response ensures adequate image quality to facilitate diagnosis and interpretation. Furthermore, the detector quantum efficiency (DQE) decreases with an increase in the x-ray energy, as do the attenuation and phase coefficients of tissue. Consequently, the use of a high energy x-ray beam is inherently disadvantageous for phase imaging in a comparison study with low energy attenuation-based clinical images. However, due to the limited output power of the micro focus x-ray tubes, a high energy x-ray beam is required for phase imaging in order to reduce the exposure times to clinically acceptable values. While we assessed the glandular dose levels for the absorbed dose to

breast tissue, the stochastic health risk such as cancer of high energy x-ray photons can be further assessed by using the equivalent dose (H_T). It is defined by the International Commission on Radiological Protection (ICRP) as the product of the absorbed tissue dose (D_T) and a weighting factor (W_R) which is related to the radiation quality. For the photon radiation like x-rays and gamma rays, the weighting factor has the value 1 independent of the energy of the radiation. Hence, the high-energy phase contrast technique does not present any higher stochastic health risk than conventional low-energy mammography technique, as compared on equal glandular dose basis.

For the 50G-50A density phantom, the observer study, contrast-to-noise ratio (CNR) and figure of merit (FOM) comparisons all indicated a large CNR improvement by the phase retrieved image as compared to both clinical systems acquired under their AEC modes at similar dose levels. The CNR improvement in the phase retrieved image was sufficient to detect the smallest discs that were undetectable by both clinical systems. With a double dose, the detectability of the discs improved due to the noise reduction provided by the system under its CNT mode. As compared to the phase sensitive image, double dose provided improved contrast resolution for the 2 mm and 1 mm disks. The clinical systems had to increase the dose to provide adequate image quality for the denser phantom. With our system, we were able to maintain the image quality enhancement without increasing the dose to the denser phantom. Thus, the comparison of 70G-30A phantom is more significant, since the phase images were acquired at a reduced relative dose as compared to the AEC mode clinical images, yet still provide a noticeable image quality enhancements in terms of the disks perception, CNR and FOM values. At double dose, the contrast resolution of the GE system for the 3 mm and 0.5 mm disks improved as compared to the phase sensitive image. For detectors with small components of additive noise, where the majority of noise is a result of x-ray quantum fluctuations, the ratio of squared CNR to exposure is essentially independent of the exposure level; thus, FOM would be expected to be a measure of performance that would not change with incident exposure.

Under the AEC acquisition mode of the GE system, the small disc diameters (0.5 and 0.25 mm) for the 50G-50A image were slightly better perceived by the observers than that of the 70G-30A image. With the CNT, the observer study indicated that the discs with diameter of 2, 1, 0.5 and 0.25 mm of the 50G-50A image were more distinguishable as compared to the 70G-30A image. For example, the 2 mm diameter disks produced an average scores of 0.233 and 0.344 with the 50G-50A and 70G-30A images. With the phase sensitive system, the 50G-50A images produced slightly higher scores for all the discs as compared to the 70G-30A image. Furthermore, the observer study indicate that the AEC mode images acquired with the Hologic system had higher disk perceptibility and detection as compared to AEC mode images of the GE system. The pixel pitch of the GE system is larger that results in reduced noise levels and less standard deviation among the pixel values of an ROI since it can capture more incident number of photons. Thus, the GE system produced similar CNR values and thus high FOM as that of the Hologic system at low radiation dose levels.

Due to technical difficulty and high cost of inserting dense CD objects in the breast phantom slabs, the CD array of holes were used. As opposed to real masses in a breast, the holes in our phantom are less attenuating than the background. Nevertheless, the CD objects like

these still provide useful differential contrast for reader preference and perception studies and CNR analyses. In the near future, we intend to a use high power micro focus x-ray source to potentially reduce the exposure time to a fraction of a second for diagnostic applications. The potential demonstrated by this study for high energy phase sensitive x-ray imaging to improve lesion detection and reduce radiation dose in mammography warrants further investigation of this technique. Future studies will utilize several phantoms, including those representing more complex anatomical tissue structures of the breast.

Acknowledgments

References

1. American Cancer Society. Breast Cancer Facts & Figures 2015–2016. Atlanta, Ga: America Cancer Society; 2015.

2. Harvey JA, Bovbjerg VE. Quantitative assessment of mammographic breast density: relationship with breast cancer risk 1. Radiology. 2004 Jan; 230(1):29–41. [PubMed: 14617762]

3. Boyd NF, Rommens JM, Vogt K, Lee V, Hopper JL, Yaffe MJ, Paterson AD. Mammographic breast density as an intermediate phenotype for breast cancer. The lancet oncology. 2005 Oct 31; 6(10): 798–808. [PubMed: 16198986]

4. Boyd NF, Guo H, Martin LJ, Sun L, Stone J, Fishell E, Jong RA, Hislop G, Chiarelli A, Minkin S, Yaffe MJ. Mammographic density and the risk and detection of breast cancer. New England Journal of Medicine. 2007 Jan 18; 356(3):227–36. [PubMed: 17229950]

5. Boyd NF, Byng JW, Jong RA, Fishell EK, Little LE, Miller AB, Lockwood GA, Tritchler DL, Yaffe MJ. Quantitative classification of mammographic densities and breast cancer risk: results from the Canadian National Breast Screening Study. Journal of the National Cancer Institute. 1995 May 3; 87(9):670–5. [PubMed: 7752271]

6. Martin LJ, Boyd NF. Mammographic density. Potential mechanisms of breast cancer risk associated with mammographic density: hypotheses based on epidemiological evidence. Breast Cancer Research. 2008 Jan 9.10(1):201. [PubMed: 18226174]

7. Li T, Sun L, Miller N, Nicklee T, Woo J, Hulse-Smith L, Tsao MS, Khokha R, Martin L, Boyd N. The association of measured breast tissue characteristics with mammographic density and other risk factors for breast cancer. Cancer Epidemiology and Prevention Biomarkers. 2005 Feb 1; 14(2):343–9.

8. McCormack VA, dos Santos Silva I. Breast density and parenchymal patterns as markers of breast cancer risk: a meta-analysis. Cancer Epidemiology and Prevention Biomarkers. 2006 Jun 1; 15(6): 1159–69.

9. American College of Radiology. BI-RADS Committee. American College of Radiology. Breast imaging reporting and data system. American College of Radiology; 1998.

10. D'orsi, CJ., Mendelson, EB., Ikeda, DM. Breast imaging reporting and data system: ACR BI-RADS—breast imaging atlas. Reston, VA: American College of Radiology; 2003.

11. Rosenberg RD, Hunt WC, Williamson MR, Gilliland FD, Wiest PW, Kelsey CA, Key CR, Linver MN. Effects of age, breast density, ethnicity, and estrogen replacement therapy on screening mammographic sensitivity and cancer stage at diagnosis: review of 183,134 screening mammograms in Albuquerque, New Mexico. Radiology. 1998 Nov; 209(2):511–8. [PubMed: 9807581]

12. Kolb TM, Lichy J, Newhouse JH. Comparison of the performance of screening mammography, physical examination, and breast us and evaluation of factors that influence them: An analysis of 27,825 patient evaluations 1. Radiology. 2002 Oct; 225(1):165–75. [PubMed: 12355001]

13. Berg WA, Zhang Z, Lehrer D, Jong RA, Pisano ED, Barr RG, Böhm-Vélez M, Mahoney MC, Evans WP, Larsen LH, Morton MJ. Detection of breast cancer with addition of annual screening ultrasound or a single screening MRI to mammography in women with elevated breast cancer risk. Jama. 2012 Apr 4; 307(13):1394–404. [PubMed: 22474203]

14. Byrne C, Schairer C, Wolfe J, Parekh N, Salane M, Brinton LA, Hoover R, Haile R. Mammographic features and breast cancer risk: effects with time, age, and menopause status. Journal of the National Cancer Institute. 1995 Nov 1; 87(21):1622–9. [PubMed: 7563205]

15. Kriege M, Brekelmans CT, Boetes C, Besnard PE, Zonderland HM, Obdeijn IM, Manoliu RA, Kok T, Peterse H, Tilanus-Linthorst MM, Muller SH. Efficacy of MRI and mammography for breast-cancer screening in women with a familial or genetic predisposition. New England Journal of Medicine. 2004 Jul 29; 351(5):427–37. [PubMed: 15282350]

16. Lee CH, Dershaw DD, Kopans D, Evans P, Monsees B, Monticciolo D, Brenner RJ, Bassett L, Berg W, Feig S, Hendrick E. Breast cancer screening with imaging: recommendations from the Society of Breast Imaging and the ACR on the use of mammography, breast MRI, breast ultrasound, and other technologies for the detection of clinically occult breast cancer. Journal of the American college of radiology. 2010 Jan 31; 7(1):18–27. [PubMed: 20129267]

17. Brem RF, Tabár L, Duffy SW, Inciardi MF, Guingrich JA, Hashimoto BE, Lander MR, Lapidus RL, Peterson MK, Rapelyea JA, Roux S. Assessing improvement in detection of breast cancer with three-dimensional automated breast US in women with dense breast tissue: the SomoInsight Study. Radiology. 2014 Oct 17; 274(3):663–73. [PubMed: 25329763]

18. Brem RF, Tabár L, Duffy SW, Inciardi MF, Guingrich JA, Hashimoto BE, Lander MR, Lapidus RL, Peterson MK, Rapelyea JA, Roux S. Assessing improvement in detection of breast cancer with three-dimensional automated breast US in women with dense breast tissue: the SomoInsight Study. Radiology. 2014 Oct 17; 274(3):663–73. [PubMed: 25329763]

19. Bravin A, Coan P, Suortti P. X-ray phase-contrast imaging: from pre-clinical applications towards clinics. Physics in medicine and biology. 2012 Dec 10.58(1):R1. [PubMed: 23220766]

20. Wu X, Liu H. Clarification of aspects in in-line phase-sensitive x-ray imaging. Medical Physics. 2007 Feb 1; 34(2):737–43. [PubMed: 17388191]

21. Wu X, Liu H. Clinical implementation of x-ray phase-contrast imaging: Theoretical foundations and design considerations. Medical physics. 2003 Aug 1; 30(8):2169–79. [PubMed: 12945983]

22. Pogany A, Gao D, Wilkins SW. Contrast and resolution in imaging with a micro focus x-ray source. Review of Scientific Instruments. 1997 Jul; 68(7):2774–82.

23. Wilkins SW, Gureyev TE, Gao D, Pogany A, Stevenson AW. Phase-contrast imaging using polychromatic hard X-rays. Nature. 1996 Nov 28.384(6607):335.

24. Wong MD, Yan A, Ghani M, Li Y, Fajardo L, Wu X, Liu H. Dose and detectability improvements with high energy phase sensitive x-ray imaging in comparison to low energy conventional imaging. Physics in medicine and biology. 2014 Apr 15.59(9):N37. [PubMed: 24732108]

25. Wu D, Yan A, Li Y, Wong MD, Zheng B, Wu X, Liu H. Characterization of a high-energy in-line phase contrast tomosynthesis prototype. Medical physics. 2015 May 1; 42(5):2404–20. [PubMed: 25979035]

26. Wu X, Yan A. Phase retrieval from one single phase contrast x-ray image. Optics express. 2009 Jun 22; 17(13):11187–96. [PubMed: 19550519]

27. Wu X, Liu H, Yan A. X-ray phase-attenuation duality and phase retrieval. Optics letters. 2005 Feb 15; 30(4):379–81. [PubMed: 15762434]

28. Wu X, Liu H, Yan A. Robustness of a phase-retrieval approach based on phase-attenuation duality. Journal of X-Ray Science and Technology. 2007 Jan 1; 15(2):85–95.

29. Wu X, Yan A, Liu H. X-ray phase-shifts-based method of volumetric breast density measurement. Medical physics. 2012 Jul 1; 39(7):4239–44.

30. Ghani MU, Yan A, Wong MD, Li Y, Ren L, Wu X, Liu H. Low dose high energy x-ray in-line phase sensitive imaging prototype: Investigation of optimal geometric conditions and design parameters. Journal of X-ray science and technology. 2015 Jan 1; 23(6):667–82. [PubMed: 26756405]

31. Boone JM. Normalized glandular dose (DgN) coefficients for arbitrary x-ray spectra in mammography: Computer-fit values of Monte Carlo derived data. Medical physics. 2002 May 1; 29(5):869–75. [PubMed: 12033583]

32. Wu X, Gingold EL, Barnes GT, Tucker DM. Normalized average glandular dose in molybdenum target-rhodium filter and rhodium target-rhodium filter mammography. Radiology. 1994 Oct; 193(1):83–9. [PubMed: 8090926]

33. Wu X, Barnes GT, Tucker DM. Spectral dependence of glandular tissue dose in screen-film mammography. Radiology. 1991 Apr; 179(1):143–8. [PubMed: 2006265]

34. Sobol WT, Wu X. Parametrization of mammography normalized average glandular dose tables. Medical physics. 1997 Apr 1; 24(4):547–54. [PubMed: 9127307]

35. Lee PC. Phase retrieval method for in-line phase contrast x-ray imaging and denoising by regularization. Optics express. 2015 Apr 20; 23(8):10668–79. [PubMed: 25969105]

36. Liu H, Wu X, Xiao T. Technical Note: Synchrotron-based high-energy x-ray phase sensitive microtomography for biomedical research. Medical physics. 2015 Oct 1; 42(10):5595–603. [PubMed: 26429234]

37. Lee, PC., Shen, HH. A study of denoising methods for in-line single distance phase image. InBiomedical Imaging (ISBI), 2015 IEEE 12th International Symposium on; 2015 Apr 16; IEEE; p. 490-493.

38. Izadifar Z, Honaramooz A, Wiebe S, Belev G, Chen X, Chapman D. Low-dose phase-based X-ray imaging techniques for in situ soft tissue engineering assessments. Biomaterials. 2016 Mar 31.82:151–67. [PubMed: 26761779]

39. Liu H, Fajardo LL, Barrett JR, Baxter RA. Contrast-detail detectability analysis: comparison of a digital spot mammography system and an analog screen-film mammography system. Academic Radiology. 1997 Mar 1; 4(3):197–203. [PubMed: 9084777]

40. Bushberg, JT., Boone, JM. The essential physics of medical imaging. Lippincott Williams & Wilkins; 2011 Dec 20.

41. Berns EA, Hendrick RE, Cutter G. Performance comparison of full-field digital mammography to screen–film mammography in clinical practice. Medical physics. 2002 May 1; 29(5):830–4. [PubMed: 12033579]

42. Suryanarayanan S, Karellas A, Vedantham S, Ved H, Baker SP, D'Orsi CJ. Flat-Panel Digital Mammography System: Contrast-Detail Comparison between Screen-Film Radiographs and Hard-Copy Images 1. Radiology. 2002 Dec; 225(3):801–7. [PubMed: 12461264]

43. Marshall NW. A comparison between objective and subjective image quality measurements for a full field digital mammography system. Physics in medicine and biology. 2006 Apr 27.51(10): 2441. [PubMed: 16675862]

44. Rose, A. Vision: human and electronic. Springer Science & Business Media; 2013 Jun 29.

45. Liu H, Karellas A, Moore SC, Harris LJ, D'Orsi CJ. Lesion detectability considerations for an optically-coupled CCD x-ray imaging system. IEEE transactions on nuclear science. 1994 Aug; 41(4):1506–9.

46. Hendrick, RE. Breast MRI: fundamentals and technical aspects. Springer Science & Business Media; 2007 Dec 14.

47. Boone JM, Seibert JA. A figure of merit comparison between bremsstrahlung and monoenergetic x-ray sources for angiography. Journal of X-ray Science and Technology. 1994 Dec 1; 4(4):334–45. [PubMed: 21307470]
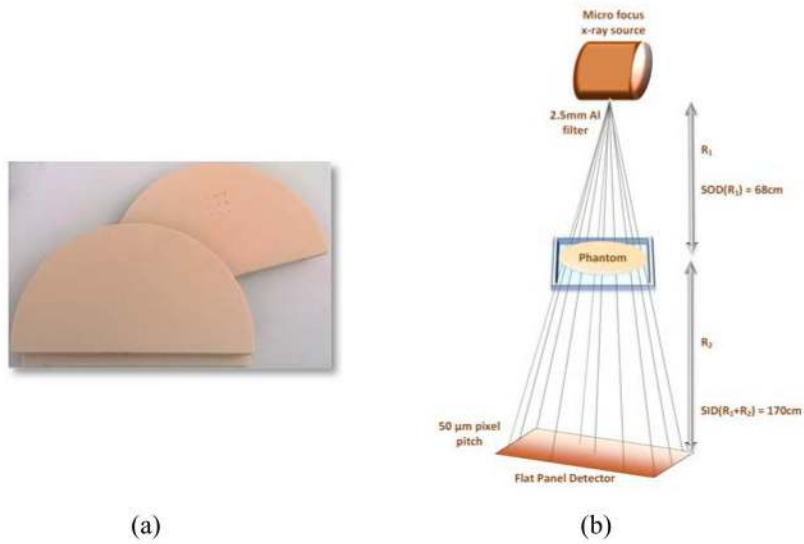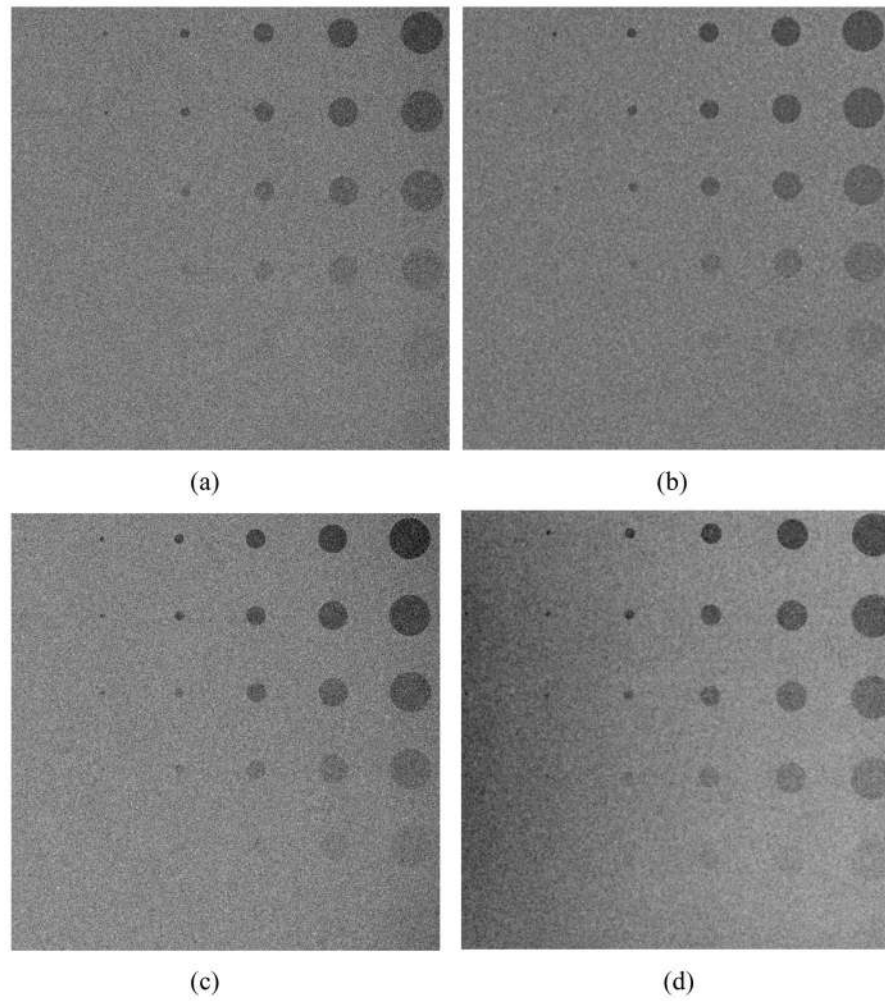
Figure 1.
(a) A 5 cm thick modular phantom mimicking the 70% glandular and 30% adipose breast tissue with the middle slab showing the CD test pattern; (b) Schematics of the inline phase sensitive x-ray imaging prototype illustrating a micro-focus x-ray source, a flat panel detector and a phantom placed in a magnification geometry.
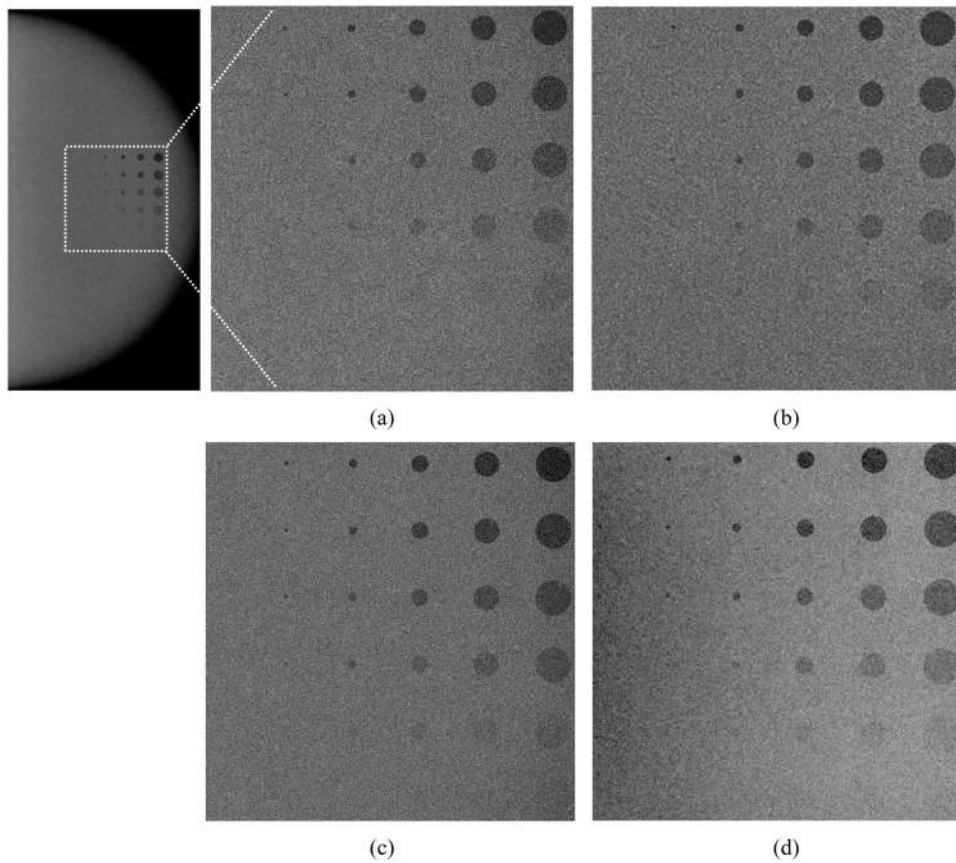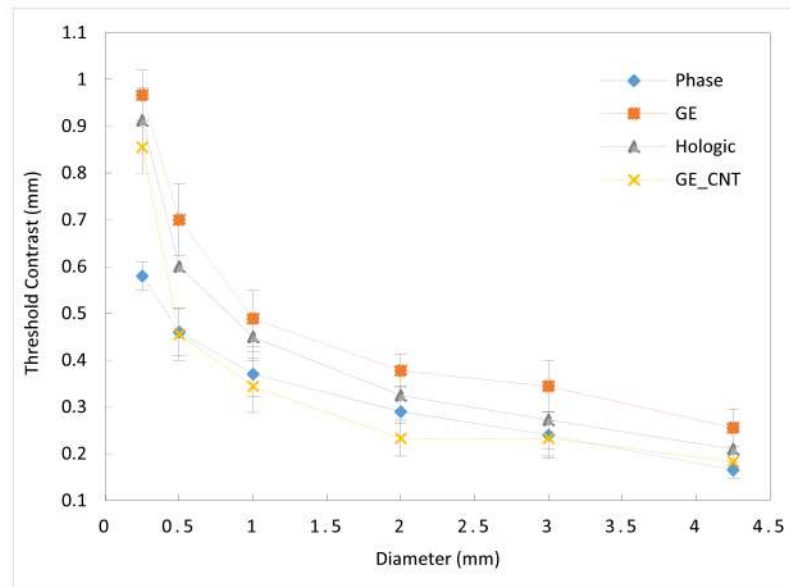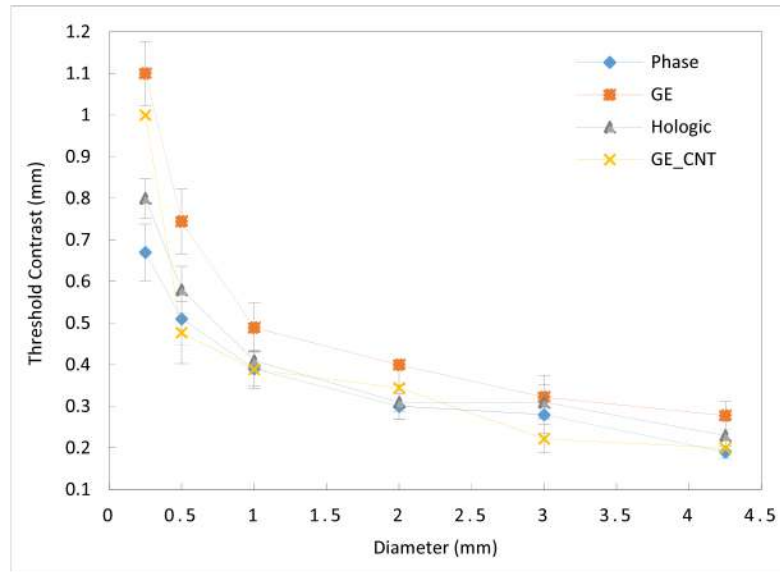
Figure 2.
CD images of 50G-50A phantom set acquired by (a) GE system at 29 kV, 46 mAs, 1.03 mGy; (b) Hologic system at 29 kV, 116 mAs, 1.42 mGy; (c) GE system at 27 kV, 146 mAs, 2.46 mGy; (d) Phase retrieved imaged acquired at 120 kV, 500 μA, 9s (4.5 mAs), 1.33 mGy.

Figure 3.
CD images of the 70G-30A phantom set acquired by (a) GE system at 29 kV, 55 mAs, 1.14 mGy; (b) Hologic system at 29 kV, 142 mAs, 1.57 mGy; (c) GE system at 28 kV, 129 mAs, 2.3 mGy; (d) Phase retrieved image acquired at 120 kV, 500 µA, 9s (4.5 mAs), 1.3 mGy.

Figure 4.
Contrast detail curve comparison of the phase retrieved image with the clinical mammography systems under various imaging protocols for the 50% glandular- 50% adipose phantom.

Figure 5.
Contrast detail curve comparison of the phase retrieved image with the clinical mammography systems under various imaging protocols for the 70% glandular- 30% adipose phantom.

Table 1

Parameters used for the acquisition of the phantoms with Senographe and Selenia.

Density	GE Senographe (G)	Hologic Selenia (H)	GE Senographe (CNT)	Phase Sensitive System
50G-50A	29kV,46mAs,1.03mGy	29kV,116mAs,1.42mGy	27kV,146mAs,2.46mGy	120kV,4.5mAs, 1.33mGy
70G-30A	29kV,55mAs,1.14mGy	29kV,142mAs,1.57mGy	28kV,129mAs,2.3mGy	120kV,4.5mAs, 1.3mGy

Table 2

Comparison of the CNR and FOM ratios of the phase retrieved image with conventional mammography systems, Hologic (H) and GE (G), for the 50% Glandular- 50% Adipose phantom set.

	CNR (P)	CNR (H)	CNR (G)	FOM(P) / FOM(H)	FOM(P) / FOM(G)
4.25mm×1mm	8.75	1.72	1.76	27.62	19.18
4.25mm×0.8mm	6.57	1.34	1.45	25.75	15.90
3mm×1mm	8.37	1.81	1.67	22.90	19.5
3mm×0.8mm	6.97	1.35	1.32	28.53	21.6

Table 3

Comparison of the CNR and FOM ratios of the phase retrieved image with conventional mammography systems, Hologic (H) and GE (G), for the 70% Glandular- 30% Adipose phantom set.

	CNR (P)	CNR (H)	CNR (G)	FOM(P) / FOM(H)	FOM(P) / FOM(G)
4.25mm×1mm	8.30	1.76	1.76	26.85	19.50
4.25mm×0.8mm	6.87	1.52	1.50	24.67	18.39
3mm×1mm	8.77	1.77	1.71	29.64	23.06
3mm×0.8mm	6.36	1.59	1.44	19.32	17.10